Boxberger, T., Pilz, M., Parolai, S. (2017): Shear wave velocity versus quality factor: results from seismic noise recordings. - *Geophysical Journal International*, *210*, 2, pp. 660—670.

DOI: http://doi.org/10.1093/gji/ggx161

Geophysical Journal International

Geophys. J. Int. (2017) **210,** 660–670
Advance Access publication 2017 April 26
GJI Seismology

doi: 10.1093/gji/ggx161

Shear wave velocity versus quality factor: results from seismic noise recordings

Tobias, Boxberger,[1] Marco Pilz[2] and Stefano Parolai[1]

[1] *Helmholtz Center Potsdam—GFZ German Research Center for Geosciences, Helmholtzstr.* 7, 14467 *Potsdam, Germany. E-mail: tobibo@gfz-potsdam.de*
[2] *Swiss Seismological Service, Swiss Federal Institute of Technology, Sonneggstr.* 5, 8092 *Zurich, Switzerland*

Accepted 2017 April 24. Received 2017 April 19; in original form 2016 July 27

SUMMARY

The assessment of the shear wave velocity (v_s) and shear wave quality factor (Q_s) for the shallow structure below a site is necessary to characterize its site response. In the past, methods based on the analysis of seismic noise have been shown to be very efficient for providing a sufficiently accurate estimation of the v_s versus depth at reasonable costs for engineering seismology purposes. In addition, a slight modification of the same method has proved to be able to provide realistic Q_s versus depth estimates. In this study, data sets of seismic noise recorded by microarrays of seismic stations in different geological environments of Europe and Central Asia are used to calculate both v_s and Q_s versus depth profiles. Analogous to the generally adopted approach in seismic hazard assessment for mapping the average shear wave velocity in the uppermost 30 m (v_{s30}) as a proxy of the site response, this approach was also applied to the quality factor within the uppermost 30 m (Q_{s30}). A slightly inverse correlation between both parameters is found based on a methodological consistent determination for different sites. Consequently, a combined assessment of v_s and Q_s by seismic noise analysis has the potential to provide a more comprehensive description of the geological structure below a site.

Key words: Seismic attenuation; Seismic noise; Site effects; Surface waves and free oscillations.

1 INTRODUCTION

The reliable assessment of seismic risk at urban scales, which is necessary for effective urban planning and the preparation of rapid response in case of a disaster, requires a trustworthy assessment of all its main components, namely, seismic hazard, seismic vulnerability and exposure. Seismic hazard assessment at the local scale needs to consider local variations of earthquake-induced ground motion resulting from lateral changes in the near-surface geology (i.e. site effects). Site effects, when earthquake recordings are lacking, can be estimated via numerical simulations once the shear wave velocity (v_s) and the shear wave quality factor (Q_s) below the investigated site are known (e.g. Parolai 2012). These parameters can be obtained either by conventional seismic methods (reflection, refraction, cross-hole, downhole, etc.), and/or by passive sources. In particular, the latter method, based on recordings of seismic noise (see, e.g. Aki 1957; Okada 2003; Parolai *et al.* 2005; Boxberger *et al.* 2011; Foti *et al.* 2011), has several advantages over conventional methods as it does not require the use of artificial sources or the drilling of boreholes, both of which are expensive and cost effective only for restricted investigation depths (a few tens of metres), and difficult to carry out in urban or environmentally sensitive areas.

While passive techniques for determining v_s are well established, on the contrary, the assessment of attenuation structure has attracted less attention, probably due to the difficulties in accurately constraining it from the seismic data. However, if the medium is not perfectly elastic (as is the case for the Earth), all seismic waves will lose energy due to the attenuation caused by the combined effects of the geometrical spreading, the frequency-dependent scattering and transmission and frequency-independent intrinsic attenuation along the transmission path due to the medium's anelasticity (Aki & Chouet 1975). Therefore, depending on the relative contribution of the different mechanism, apparent attenuation will also be frequency-dependent. Correspondingly, the mapped quality factor Q_{app}, which is an apparent quality factor, indicates, simply stated, the loss of energy of a single wavelength arising from the various mechanisms of attenuation at various scales due to the combined effect of the intrinsic and scattering quality factors, Q_i and Q_{sc}, respectively,

$$\frac{1}{Q_{app}} = \frac{1}{Q_i} + \frac{1}{Q_{sc}}. \quad (1)$$

So far, most of the relevant studies on Q in the shallow unconsolidated materials within the framework of energy reduction studies

have relied on borehole data (e.g. Assimaki *et al.* 2006; Parolai *et al.* 2010), while some attempts have been made using active seismic source generated surface waves (e.g. Xia *et al.* 2002). Recently, Prieto *et al.* (2009) showed that it is possible, at the regional scale, to estimate the attenuation of surface waves using seismic noise recordings. They also inverted for the 1-D Q_s structure, showing that the method can be adapted for regionalized comparisons of distinct regions or large-scale structural features. Similarly, Weemstra *et al.* (2012) estimated the attenuation and quality factor of surface waves using recordings from an array with an aperture of several kilometres but did not attempt any Q_s 1-D inversions. In terms of more local scales, Albarello & Baliva (2009) estimated the damping in soil of surface waves by seismic noise measurements, but again, did not estimate Q_s. It should be noted that the distribution of noise sources has been found to have a significant effect on the behaviour of the azimuthally averaged coherence, which is generally used for estimating attenuation (Tsai 2011; Weaver 2011).

While Prieto *et al*. (2009) model their spatial coherence results by including an exponential decay function which is associated with the propagation time between the sources and stations, Weemstra *et al*. (2014) showed that the approximation of fitting a downscaled, decaying Bessel function will only result in significant error in the attenuation estimates at relatively small inter-receiver distances. Other studies (e.g. Cupillard & Capdeville 2010; Cupillard *et al.* 2011) demonstrate theoretically that surface wave attenuation can be retrieved from noise correlations if there is an azimuthally and radially uniform distribution of noise sources. Liu & Ben-Zion (2013) showed that the interstation attenuation might cause additional amplitude reduction, which is non-exponential and related to properties of frequency-domain Struve functions. Based thereon, Liu *et al*. (2015) were able to develop an inversion algorithm to identify the effects of attenuation on noise cross-correlation between pairs of stations in a model with separate interstation Q value from that of the background attenuation. Moreover, for a very dense array, Bowden *et al*. (2015) presented a 2-D wave front tracking approach which offers the potential of spatially resolving intrinsic attenuation and scattering if the noise wavefield is sufficiently omnidirectional.

Recently, it was suggested that the extended spatial autocorrelation method (Ohori *et al*. 2002) method can provide, with just a few additional calculation steps, realistic Q_s versus depth estimations (Parolai 2014) also at local scales (a few tens of metres), therefore indicating that seismic noise analysis has the potential to provide a more comprehensive (in terms of both v_s and Q_s) description of the geological structure below a site. However, the method requires extensive testing before being adopted for geotechnical applications.

In this study, analogous to the generally adopted approach in seismic hazard assessment for mapping the average shear wave velocity in the uppermost 30 m (v_{s30}) as a proxy for site response, we will focus on the quality factor within the uppermost 30 m (Q_{s30}). Based thereon, efforts are made to (1) improve and further test the method proposed by Parolai (2014) in combination with the approach of Boxberger *et al*. (2011) that aimed at better constraining the subsoil structure by the joint inversion of Rayleigh, Love dispersion and horizontal-to-vertical spectral ratio curves, (2) to evaluate, based on a data set of homogeneously estimated quality factors, if a possible link between velocity and Q_s variation might exist which would allow the damping factor to be estimated at sites where only velocity values are available and (3) if yes, to the previous point, to investigate the physical reason behind such a link.

2 METHOD

The space correlation function (ω) introduced by Aki (1957) for the vertical component of seismic noise data can be written as (Ohori *et al.* 2002)

$$\bar{\rho}_{jn}(\omega) = \frac{\frac{1}{M}\sum_{l=1}^{M} \mathrm{Re}({}_m S_{jn}(\omega))}{\sqrt{\frac{1}{M^2}\sum_{l=1_m}^{M} S_{jj}(\omega)\sum_{l=1_m}^{M} S_{nn}(\omega)}} \tag{2}$$

where ${}_{\mathrm{m}}S_{\mathrm{jn}}$ is the cross-spectrum for the mth segment between the jth and mth stations, M is the total number of segments, ${}_{\mathrm{m}}S_{\mathrm{jj}}$ and ${}_{\mathrm{m}}S_{\mathrm{nn}}$ are the power spectra of the mth segment at stations j and n, respectively and ω corresponds to the angular frequency.

As discussed by Aki (1965), the spatial autocorrelation equations derived for the analysis of the vertical component of ground motion can, in principle, be adapted for the analysis of the horizontal components, with the aim of extracting the phase velocities of Rayleigh and Love waves. In fact, in the case of Rayleigh waves, when they are polarized parallel to the propagation direction, equations similar to eq. (2) can be derived for both the radial and tangential components of motion (see Boxberger *et al.* 2011 for details).

If the space-correlation function is calculated for a single angular frequency ω_0 and normalized to the power spectrum, it can be expressed in the form

$$\bar{\rho}(r, \omega_0) = J_0\left(\frac{\omega_0}{c(\omega_0)} r\right), \tag{3}$$

where $c(\omega)$ is the frequency-dependent phase velocity and J_0 is the Bessel function of order zero. Eq. (3) assumes that only fundamental-mode energy is present. In the cases considered in the following, we have investigated the correctness of this assumption and we have verified that higher modes play a minor role in the dispersion curves we derived empirically. This was achieved by calculating the theoretical dispersion curves (for several modes and the apparent one) for the best-fitting S-wave velocity model calculated from the inversion of the empirical dispersion curve only. For all studied cases, the theoretical dispersion curve was shown to follow mainly the trend of the fundamental mode.

Differently from the original Aki (1965) assumption, however, realistic mediums are anelastic, meaning that the attenuation of seismic waves should take into account Q, which is directly related to the total decay of elastic energy when it spreads through a medium. The seismic attenuation presented here does not differentiate scattering from intrinsic attenuation, but Q can be considered as being a representation of the effective physical properties and state of the medium's material.

Prieto *et al*. (2009) showed that eq. (3), in order to take into account attenuation for plane waves, can be modified to be written as

$$\bar{\rho}(r, \omega_0) = J_0\left(\frac{\omega_0}{c(\omega_0)} r\right) e^{-\alpha(\omega) r}, \tag{4}$$

$$\alpha(\omega) = \frac{\omega}{2 Q_r(\omega) c(\omega)}, \tag{5}$$

Where $\alpha(\omega)$ is the frequency-dependent Rayleigh wave attenuation factor and $Q_{\mathrm{r}}(\omega)$ is the frequency-dependent quality factor for Rayleigh waves.

An iterative grid-search procedure can be applied based on eq. (4) to jointly find the values of the phase velocity and the frequency-dependent attenuation factor $\alpha(\omega)$ that give the best fit to the data which is achieved by minimizing the root-mean square (rms) of the

differences between the values calculated using eqs(2) and (4). Once the phase velocity and $\alpha(\omega)$ are known, $Q_r(\omega)$ can be estimated using eq. (5). Note that, according to Li *et al*. (1995), eq. (5) represents the phase velocity and not the group velocity since we are dealing with the spatial quality factor and not with the temporal one.

The relationship between the Rayleigh wave attenuation factor and the quality factor for P (Q_p) and S waves (Q_s) of a layered model can be written in a linear form by (Anderson *et al.* 1965; Xia *et al.* 2002; Parolai 2014)

$$\alpha(\omega) = \frac{\omega}{2c(\omega)^2}\left[\sum_{i=1}^{m} V_{pi}\frac{\partial c(\omega)}{\partial v_{pi}}Q_{pi}^{-1} + \sum_{i=1}^{m} V_{si}\frac{\partial c(\omega)}{\partial V_{si}}Q_{si}^{-1}\right], \quad (6)$$

where Q_{pi} and Q_{si} are the apparent quality factors for the P and S waves in the ith layer, respectively, v_{pi} and v_{si} are the P- and the S-wave velocities of the ith layer, respectively and m is the number of layers of a layered earth model. Since the quality factors can only assume positive values, the system is solved using a least-squares algorithm employing a positivity constraint (e.g. Menke 1989).

In general, when v_s/v_p is larger than 0.4, the attenuation coefficient dependence on Q_p is significant, meaning that Q_p cannot be disregarded (Xia *et al.* 2002). In all other cases, the inversion can be carried out only for Q_s. In these cases, eq. (6) becomes

$$\alpha(\omega) = \frac{\omega}{2c(\omega)^2}\left[\sum_{i=1}^{m} V_{s\,i}\frac{\partial c(\omega)}{\partial V_{s\,i}}Q_{s\,i}^{-1}\right]. \quad (7)$$

The partial derivatives are numerically approximated by applying a small perturbation to the initial model (Parolai *et al.*2012).

Please note that the estimates of v_s and Q_s are done separately. This means, first that the dispersion curve(s) are inverted to obtain the S-wave velocity model. Second, the inversion for the quality factor is carried out of. When inverting for Q_s, only the shallow layers, for which the Jacobian matrix shows sufficient sensitivity, is considered (see Parolai *et al*. 2012).

Note that the conjecture of an exponentially decaying Bessel function (eq. 4) is valid in a strict sense only for infinite homogeneous media having spatially uniform velocity and attenuation (Snieder 2001). Furthermore, previous studies (Cupillard & Capdeville 2010) showed that even for a laterally heterogeneous attenuation, a non-uniform distribution of noise sources could make it difficult to estimate attenuation by seismic interferometry. However, the spatial autocorrelation (SPAC) method should reduce this effect due to a heterogeneous distribution of noise sources and attenuation by taking average of many station pairs having similar separations but different azimuth angles. In this sense, although the conjecture of Prieto *et al*. (2009) cannot serve as a strict solution, it can still be seen as a good approximation, even in cases of strong attenuation as the maximum deviations have been found to be of the order of only a few per cent (Nakahara 2012).

3 DATA SETS

To allow a comparison of various shear wave velocity and shear wave quality factor profiles, data sets recorded in different regions across Europe and Central Asia were employed (Fig. 1). Generally, the measurements were carried out in urban areas on fallow land, as well as on grassland in suburban areas. At all sites, the array nodes were placed irregularly on the surface. The interstation distances were chosen as a good compromise between sufficient resolution at shallow depths (i.e. a reasonable distribution of small interstation distances between the inner stations) and the maximum depth of investigation (i.e. large interstation distances for the outermost stations). The array measurements were performed on various stratigraphic units by different numbers of stations and combinations of instruments listed in Table 1, with digitizers from Guralp, Quanterra or the GFZ–WISE (see Picozzi *et al.* 2010) connected to broad-band seismometers, short-period seismometers or geophones.

Short-period seismometers are generally adopted to cover the frequency range between ~0.2 Hz up to several tens of Hertz. Geophones are passive analog devices and typically comprise a spring-mounted magnetic mass moving within a wire coil to generate an electrical signal. The construction of a short-period sensor is similar to the geophone, but with a lower corner frequency. For a 4.5 Hz geophone, due to limitations in mechanical and electrical parameters, the recordings can be considered reliable generally only for frequencies above 1 Hz (Strollo *et al.* 2008). Due to their instrumental characteristics, short-period seismometers and 4.5 Hz geophones

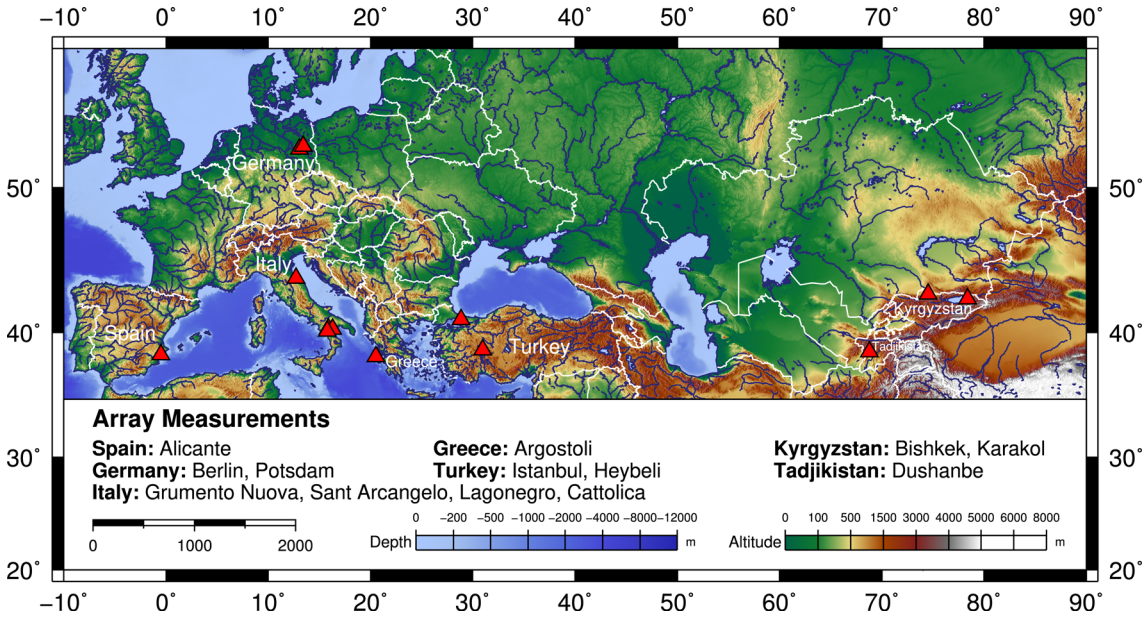

Figure 1. Location of the different microarray sites used in this study.

Table 1. Details about the array sites and instrument specification from which the data sets in this study were obtained (see Fig. 1).

Region	Site	Array specification	Stratigraphic units	Interstation distance min/max (m)
Spain	Alicante	19 station, GFZ–WISE system, 4.5 Hz geophones	Sandy clay and fines and	3.5/94
Italy	Tito	11 stations, EDL data logger, 1 s Mark L-4C-3-D sensors	Clay	5/67
	Grumento Nuova	14 stations, EDL data logger, 1 s Mark L-4C-3-D sensors	Medium dense sand and stiff clay	5/127
	Sant Arcangelo	14 stations, EDL data logger, 1 s Mark L-4C-3-D sensors	Silty clays	6/70
	Lagonegro	14 stations, EDL data logger, 1 s Mark L-4C-3-D sensors	Dense sand and gravel	3.5/102
	Cattolica	14 stations, EDL data logger, 1 s Mark L-4C-3-D sensors	Very dense sand and gravel	5/115
Greece	Argostoli	Array 1: 16 stations, EDL/Quanterradata logger, 1 s MarkL-4C-3-D/Lennarz 5 s sensors	Gravel	13/220
		Array 2: 19 stations, Guralp Data logger, Guralp CMG40T sensors	Gravel	7/260
Germany	Berlin	18 stations, GFZ–WISE system, 4.5 Hz geophones	Fine/medium sand	3/75
	Potsdam	18 stations, GFZ–WISE system, 4.5 Hz geophones	Fine/medium sand	4/45
Kyrgystan	Bishkek	Array north: 16 stations, GFZ–WISE system, 4.5 Hz geophones	Silt and loess	6/98
		Array south: 16 stations, GFZ–WISE system, 4.5 Hz geophones	Gravel and pebbles	3/142
	Karakol	20 stations, GFZ–WISE system, 4.5 Hz geophones	Pebbles	2.5/168
Tajikistan	Dushanbe	24 stations, EDL data logger, 1 s Mark L-4C-3-D sensors	Loess and clay	5/145
Turkey	Istanbul	10 stations, EDL data logger, 1 s Mark L-4C-3-D sensors	Sandy clay and sand	11.5/232
	Heybeli	17 stations, GFZ–WISE system, 4.5 Hz geophones	Sand	5.5/136

provide satisfactory results for dense array measurements over the frequency range 1–20 Hz. GFZ–WISE are low-cost digitizers developed by GFZ (Fleming *et al.* 2009; Picozzi *et al.* 2010) that are able to create wireless mesh networks, hence real-time analysis directly in the field of the data is feasible. All the instruments are appropriate for recording seismic noise in the frequency range greater than 1 Hz and it is this frequency band that is exploited for calculating v_{s30} and Q_{s30}.

At each array site, using Global Positioning System timing, the seismic noise was recorded for a minimum of 1 hr at sampling rates of 100 or 200 Hz. For calculating the spatial-correlation coefficients using eq. (2), each station´s data were divided into 120 non-overlapping 30 s windows. In order to reduce leakage problems, each signal window is tapered for 5 per cent of its length at both ends using a cosine function. The vertical and horizontal components of ground motion were used to estimate the Rayleigh and Love wave dispersion curves and the Rayleigh wave attenuation factors for all array sites. To this regard, an iterative grid-search procedure is performed based on eq. (2). In the grid-search procedure, $c(\omega)$ was varied over a very wide range between 50 and 3000 m s^{-1} in steps of 1 m s^{-1} in order to exhaustively cover all possible values of the phase velocity, while the frequency-dependent attenuation factor $\alpha(\omega)$ was varied between 0 and 0.18 m^{-1} in steps of 0.0002 m^{-1}. For every iteration step, the velocity of the Rayleigh waves is re-estimated in order to check on the possible influence of the different procedure on the phase velocity assessment. Furthermore, a selection criterion is included by considering only interstation distances less than twice the wavelength of the grid-search procedure. Once the phase velocities have been constrained, a joint inversion (Parolai *et al.* 2005; Picozzi *et al.* 2005), which combines the results of the dispersion curve and H/V estimates, is applied in order to retrieve *S*-wave velocity profiles. Different parametrizations of the velocity model were tested, and finally we selected 4–6 layers in order to avoid overparametrization.

In turn, the data kernel matrix is calculated considering both the *P*- and *S*-wave velocity contributions to the attenuation factors (eq. 6). Considering the case of a medium where the v_s/v_p ratio is much smaller than 0.4, the contribution of v_p to the attenuation factor is negligible (see, e.g. Parolai 2014). For such a medium, which was most commonly encountered during this work due to the existence of shallow water tables, the inversion accounts for the contributions of v_s and Q_s only (eq. 7). Otherwise, the general form (eq. 6) is used.

4 RESULTS

An example of the results of the grid-search procedure for obtaining the dispersion curves for the array test sites in southern Bishkek (Kyrgyz Republic) and Berlin (Germany) for eight analysed frequencies is shown in Fig. 2. The two presented array sites are representative for the entire data set as they are characterized by very different geological structures. The mapped frequencies have been chosen to provide a representative selection over the entire frequency range. As expected, for the lower frequencies, a reasonable fit of the Bessel function can be obtained, whereas for higher frequencies, the goodness of the fit generally decreases as the Bessel function cannot be fitted over the entire distance range.

The attenuation factors can be reasonably constrained, especially in the low-frequency range. This is particularly evident for the Berlin test site (Fig. 3, bottom). For increasing frequency values, the uncertainty increases since higher frequencies loose coherence faster and so are more likely to be influenced by small-scale heterogeneities, meaning that the minima become smeared along the vertical axis. On the other hand, the error functions show a predominant and very narrow minimum along the horizontal velocity axis, meaning that the phase velocity can be constrained well while the accuracy of the attenuation shows more smeared values.

By jointly inverting the H/V and the dispersion data, Fig. 4 shows that the *S*-wave velocity profile can be reliably mapped down to a depth of almost 100 m. A steady velocity increase with depth and no strong impedance contrast (i.e. a rather flat horizontal-to-vertical

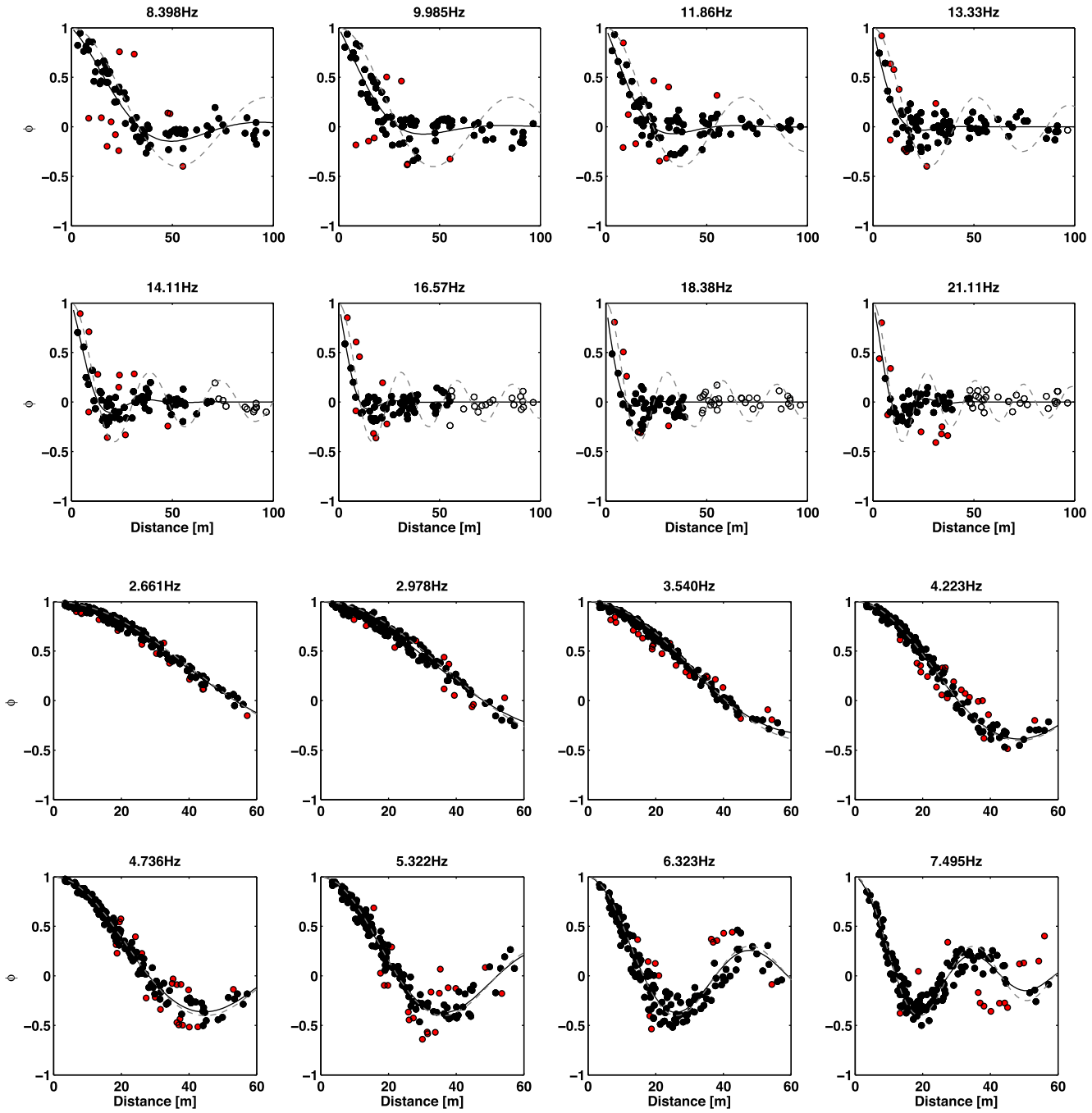

Figure 2. Measured spatial-correlation coefficients for different frequencies (black dots) and the best-fitting Bessel functions (black line) at the test site in southern Bishkek (top two rows) and Berlin (bottom rows). Red dots indicate the space-correlation values discarded by the fitting procedure. White dots indicate the space-correlation values discarded due to the wavelength criteria. The dashed lines provide a comparison with the Bessel function fit considering only $c(\omega)$ in order to make clear the improvement when including α (ω).

spectral ratio (HVSR) with no significant peak) allow the model to be well constrained for the shallow part (only small deviations) whereas for the deeper part the deviations are larger.

Fig. 5 provides an example of the attenuation factors and the estimated $Q_r(\omega)$. In general, for increasing frequency values, $\alpha(\omega)$ also increases over the entire frequency band, which hints at an almost stable, slightly increasing quality factor with depth. While this trend can clearly be recognized for the Bishkek test site (Fig. 5, top), the data for the Berlin test site (Fig. 5, bottom) are much more scattered and no clear trend can be observed.

Exploiting the minimum misfit 1-D *S*-wave velocity models shown in Fig. 4, to obtain the shear wave quality factor for each sublayer, an inversion was carried out based on eq. (7), which only accounts for the contribution of v_s and Q_s. In order to check the quality of the inversion results, the data kernel matrix was calculated (Fig. 6). While the first two (Bishkek test site) to three (Berlin test site) layers are well constrained, for the fourth layer and deeper structures, no reliable information could be obtained.

Table 2 lists the obtained v_s and Q_s values for the two representative test sites. Although for the Bishkek site the Q_s values show

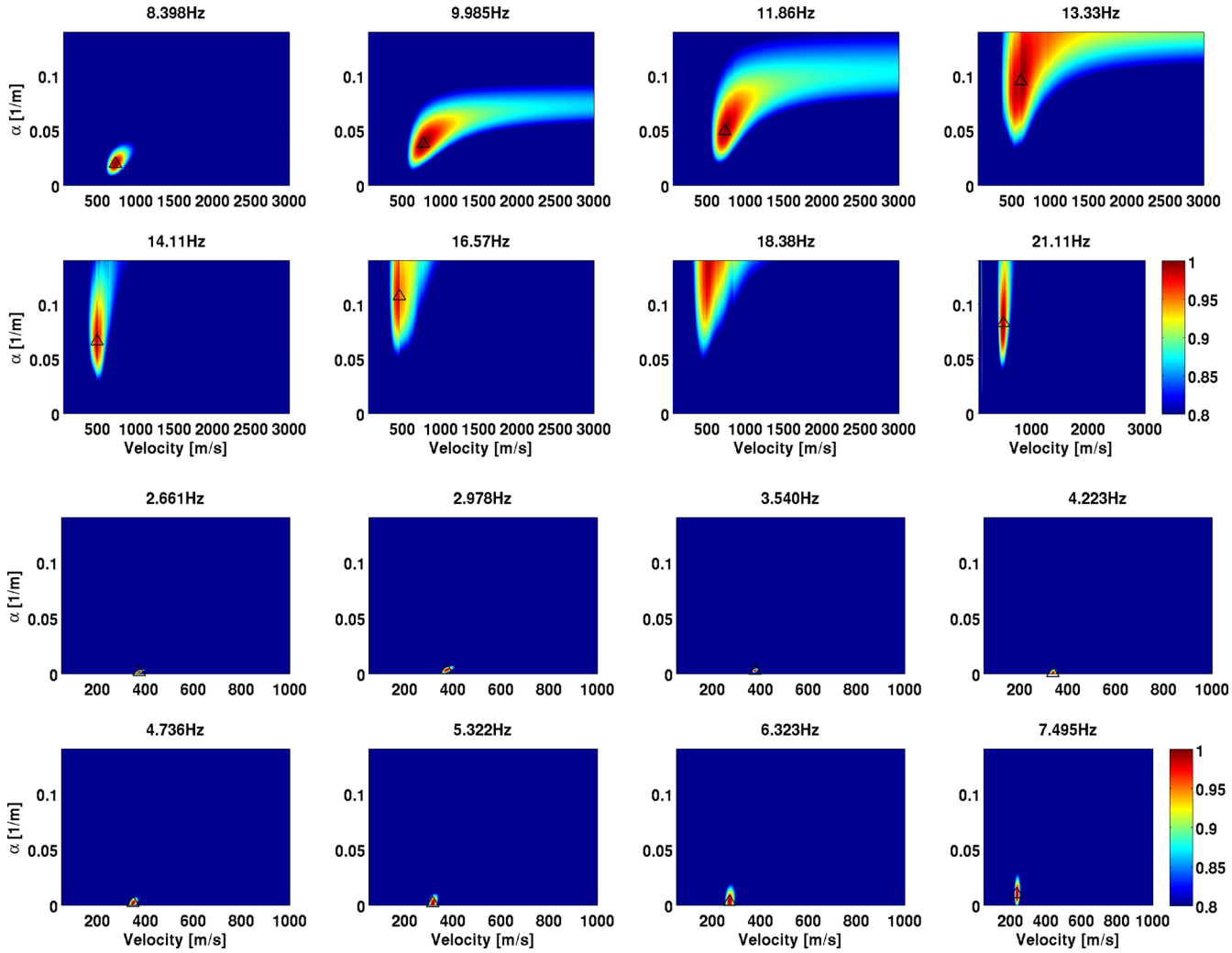

Figure 3. The normalized fit value (estimated as rms min/rms) for measurements in southern Bishkek (top two rows) and Berlin (bottom rows). White triangles indicate the $\alpha(\omega)$ and $c(\omega)$ combination that provide the best fit to the observed spatial-correlation coefficients.

rather low values, the values are larger, as expected, than those obtained for Q_r due to the smaller attenuation of body waves. The relatively high velocities in Bishkek might be related to the composition of the matrix of the pebbles-gravel deposits (see Table 1). The Berlin test site is characterized by rather thin layers having very low *S*-wave velocities and a corresponding low level of attenuation. These two test sites therefore show that higher *S*-wave velocities do not necessarily correspond to higher values of Q_s, but we even observe an opposite trend.

5 DISCUSSION

Since a generally adopted approach in seismic hazard assessment is mapping the average shear wave velocity in the uppermost 30 m, we calculate the traveltime-based average velocity in the uppermost 30 m and, correspondingly, the traveltime-based average quality factor.

A comparison of the obtained v_{s30} and Q_{s30} values for all array measurement sites is shown in Fig. 7 clustered for the stratigraphic units' clay, sand and gravel. Although there is a high level of scatter in the data (especially for v_{s30} less than 300 m s^{-1}), remarkably low apparent Q_{s30} values have been obtained for the shallow layers (even values down to 3 for the Bishkek test site, where gravel is prevalent, and at many sites lower than 10, see Fig. 7). Although such values might seem exceptional, for example Hu & Su (1999) and Ozakin & Ben-Zion (2016) have found values of a similar order of magnitude. For the Istanbul test site, such a low value of Q_{s30} is confirmed by Parolai *et al*. (2010), who found a value of Q_s of 15 for the uppermost 50 m. However, although such values might seem remarkably low, they might also represent the apparent attenuation (i.e. the combined effect of intrinsic and scattering attenuation).

As these values are derived after the inversion of the spatial autocorrelation coefficients, which are directly related to the time-domain Green's function describing the direct propagation of surface waves between the sensors of the array without considering bended ray paths (see, e.g. Yokoi & Margaryan 2008; Tsai & Moschetti 2010), it is likely that we mainly capture the intrinsic mechanism of energy loss of the direct surface waves which is likely to dominate over scattering, in agreement with large-scale crustal studies by Del Pezzo *et al*. (1995) and Tselentis (1998). The fact that the intrinsic attenuation is likely to dominate at higher frequencies in all the cases, is also in line with the results of the detrended fluctuation analysis (*cf.* Pilz & Parolai 2014) which shows mainly ballistic (i.e. less diffusive and less scattering) behaviour for most of the sites (the scattering redistributed energy is anyway correlated in the noise wavefield analysis).

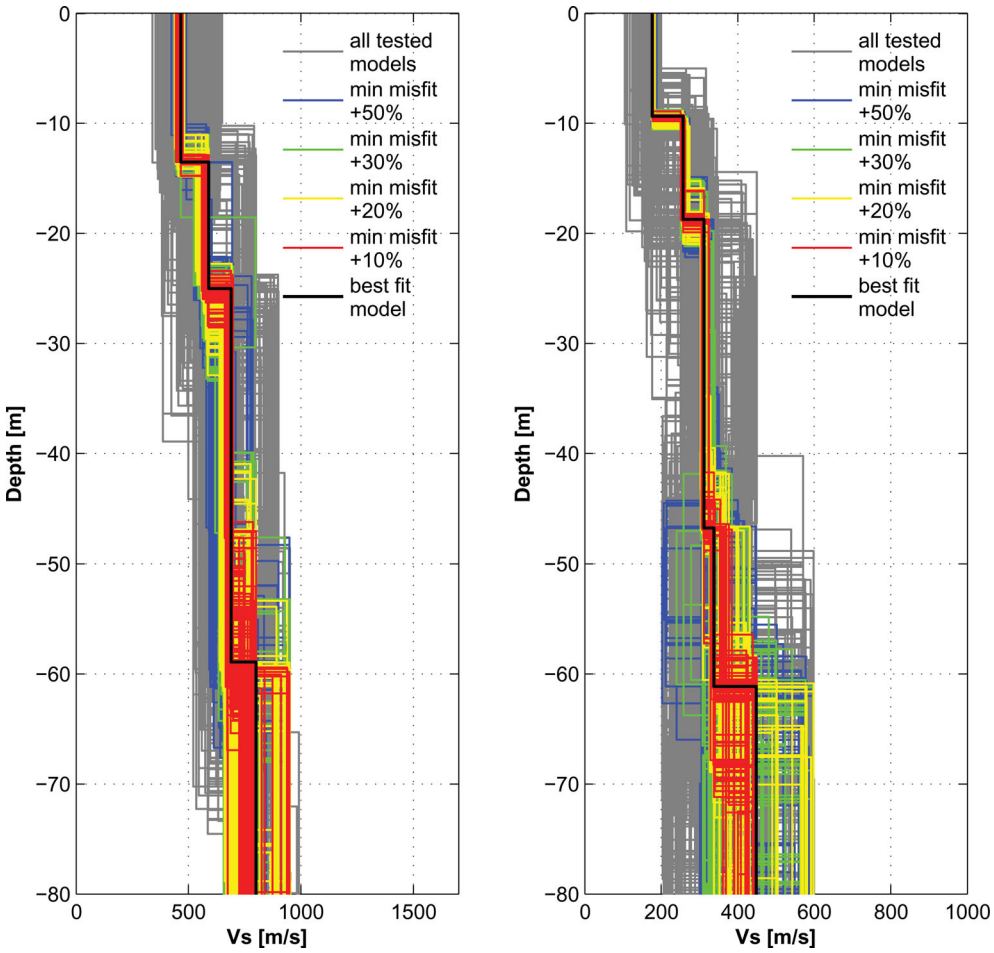

Figure 4. *S*-wave velocity profiles from the RHV joint inversion for the Bishkek (left) and Berlin (right) test sites; best-fit model (black line), models in a range of the best-fit model +10 per cent (red lines), +20 per cent (yellow lines), +30 per cent (green lines),+50 per cent (blue lines), and all models (grey lines).

Remarkably, a slight trend of decreasing Q_{s30} with increasing values of v_{s30} is found. This trend is particularly obvious for the high velocity range. Even for neighbouring array measurements (e.g. like in the case of Argostoli, Greece, stars at $v_{s30} = 500$ and 550 m s^{-1} in Fig. 7), a similar trend can be observed. These findings are apparently in contradiction to previous studies (Campbell 2009; Ktenidou *et al.* 2015). Whereas Ktenidou *et al.* (2015) observed that attenuation stabilizes for high values of v_s, Campbell (2009) suggested that attenuation generally decreases (i.e. Q_s increases) with increasing velocity.

However, in the latter study (Campbell 2009), a similar trend of decreasing Q_s with increasing v_s was observed for the range of velocities analysed in this study. Only when velocities typical of rock materials where considered, where the attenuation can take place with different mechanisms with respect to the unconsolidated material, an opposite trend can be found for the results of Campbell (2009, see Fig. 7).

Therefore, a joint analysis of soft and rock soil properties (as, e.g. recommended by Nikolaou *et al.* 2012) should probably not be carried out due to the different mechanisms that are likely to determine the attenuation of seismic waves propagating in the material (cracks opening versus particle friction at the particle contact, the role of fluids and porosity, etc.). The (weak) trend of decreasing quality factor with increasing *S*-wave velocity ($R^2 = 0.25$, see Fig. 7) might be better related to the differences in the type of material considered. In fact, for the presented examples, the higher velocities in Bishkek might explain more convincingly by the composition of the matrix of the pebbles-gravel deposits being stiffer than the sands in Berlin. On the contrary, much larger values for Q_s have been calculated for the Berlin test site. Previous studies (e.g. Vucetic & Dobry 1991) have shown that—while low *S*-wave velocities are generally found for clay and silty materials (see Table 1) with a higher plasticity index (PI)—higher velocities are expected for sandy and gravel soils (mainly saturated non-cohesionless non-plastic soil with PI low or equal to 0). This is mainly due to the greater stiffness of the grain matrix. On the other hand, the efficiency of propagation, and therefore the quality factor, is related to the contacts between the grains, which is poorer in coarse grained, sandy and gravel soils, which are more inclined to non-linear behaviour during strong shaking, than in fine grain (silt and clays) ones (e.g. Ishibashi & Zhang 1993).

In particular, Vucetic & Dobry (1988) suggested that materials with high and very high plasticity are composed of very small particles having a relatively high surface area per unit weight of the particle, and therefore having a large number of particle contacts. The electrical and chemical bonds and repulsion forces between the particles are also large compared to the weight of the particles themselves and therefore dominate the behaviour of soil skeleton under load. Sand and gravels, having low or zero plasticity, have fewer interparticle contacts, and the gravitational forces and associated friction between the grains exert a dominant role on the response

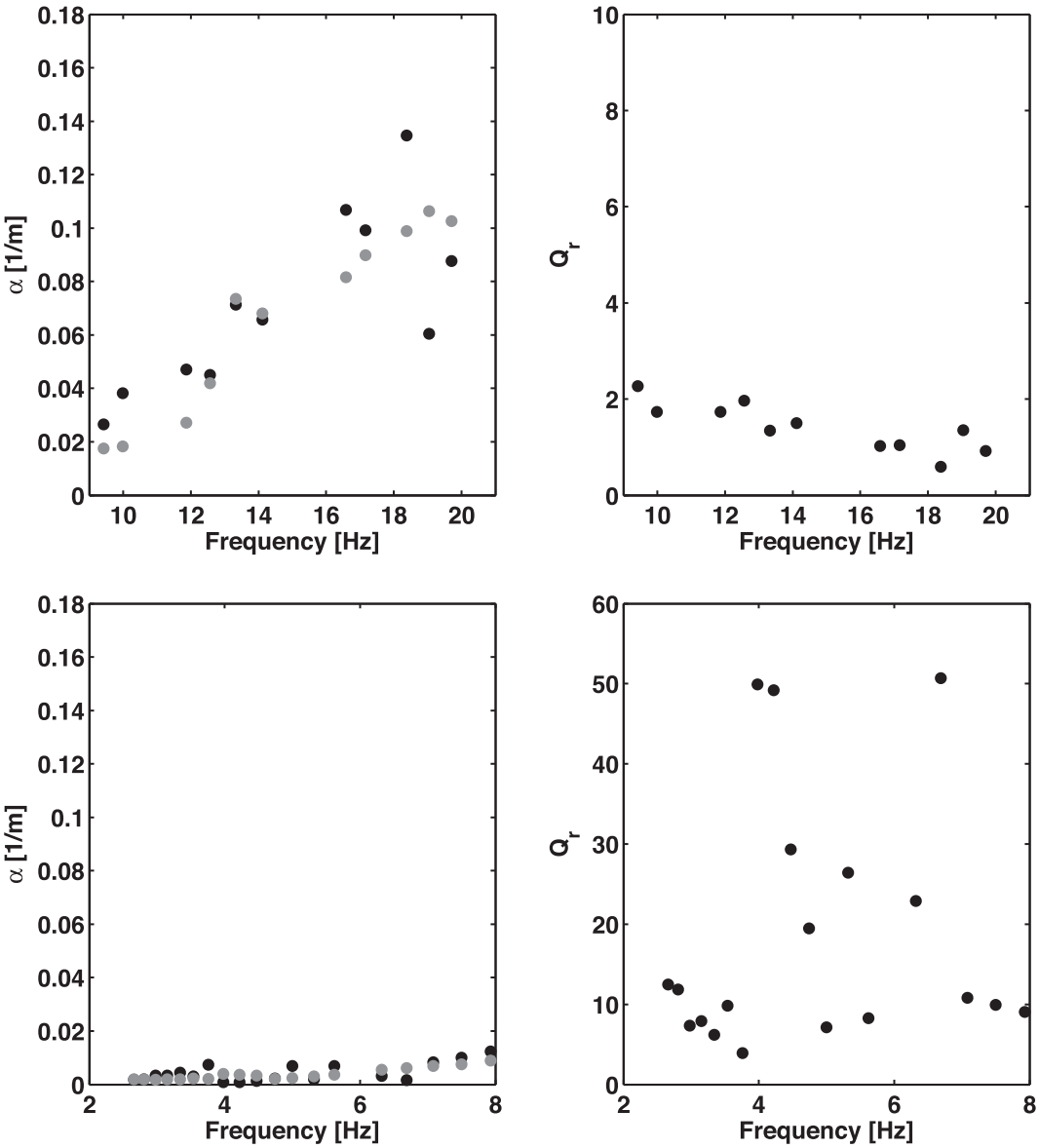

Figure 5. Left: observed attenuation factors (black circles) and retrieved attenuation factors after the inversion (grey circles). Right: Rayleigh wave quality factor Q_r for the Bishkek (top) and Berlin (bottom) test sites.

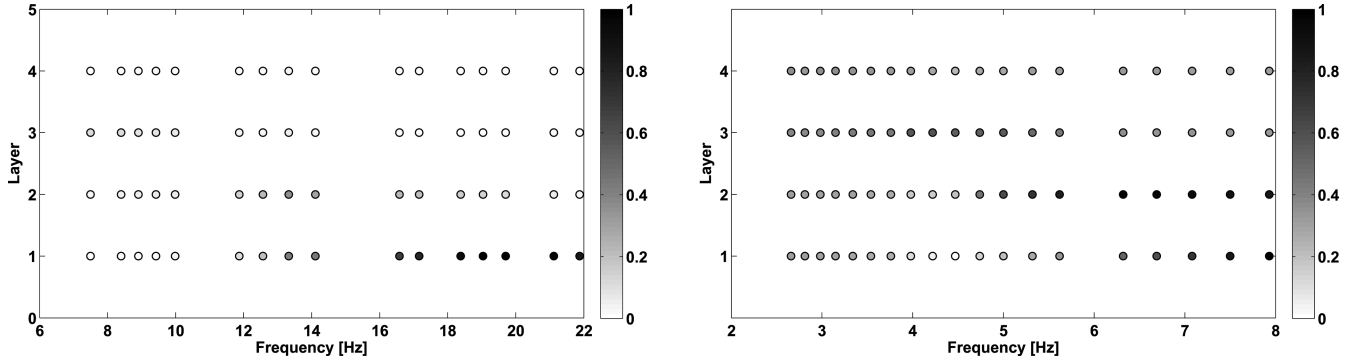

Figure 6. The data kernel matrix for the Bishkek (left) and Berlin (right) test sites. The elements are related to the dependence of the attenuation on v_s.

Table 2. Layer thickness, *S*-wave velocity and *S*-wave quality factor results for the arrays in southern Bishkek and Berlin.

Layer	Bishkek			Berlin		
	Thickness (m)	v_s (m s^{-1})	Q_s	Thickness (m)	v_s (m s^{-1})	Q_s
1	13	464	2.6	9.4	176	32.7
2	11	589	3.1	9.4	257	69.5
3	33	689	5.5	28	312	34.9
4	37	799		14.4	337	

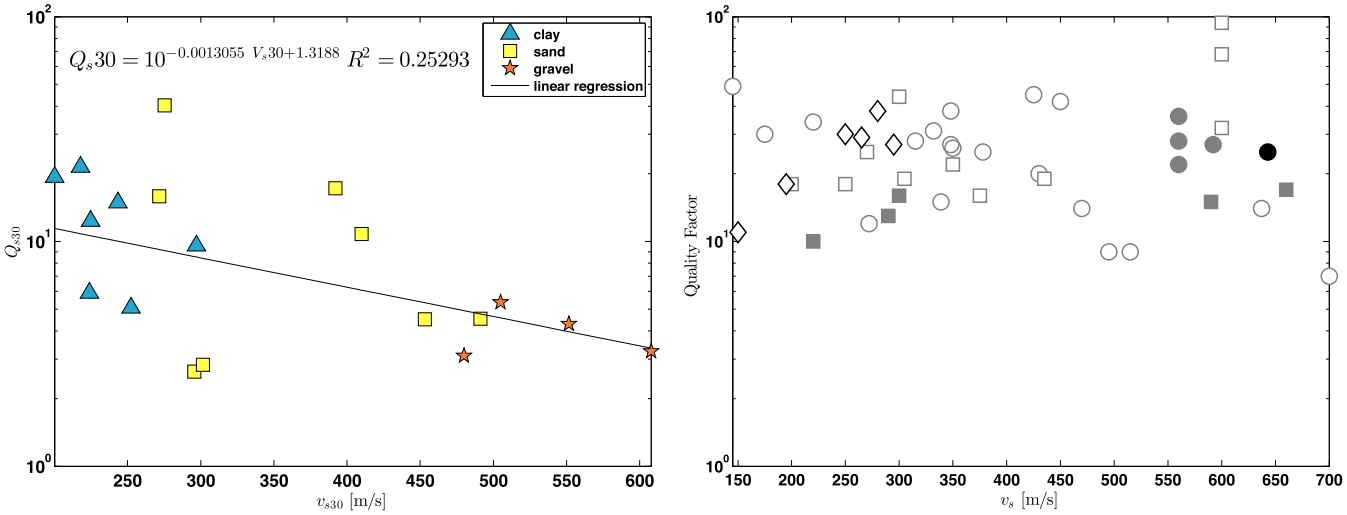

Figure 7. Left: Q_{s30} versus v_{s30} for all studied microarray sites clustered around stratigraphic units (see Table 1) with linear regression. Right: Q_{s30} versus v_{s30} of the study of Campbell (2009). Gray solid circles: sedimentary profiles in ENA and Uzbekistan derived from weak-motion recordings. Gray solid squares: profiles from boreholes in California derived from weak-motion recordings. Gray open squares: unconsolidated sedimentary soils of the Mississippi Embayment. Gray open circles: near-surface unconsolidated soils in California. Gray open diamonds: laboratory measurements on specimens of unconsolidated sediments and hard sandstone.

to external loads. They therefore suggested that the microstructural bonds and repulsion forces in the higher plasticity soils act like a system of relatively flexible springs that have the ability to take relatively large shear strains before the particles are permanently displaced and non-linear and stiffness degradation effects start appearing. On the other hand, they highlighted how in low plasticity soils, the only source of linear behaviour is the elasticity of the particles, explaining why non-linear and stiffness degradation starts in these soils at low strains.

However, Dobry & Vucetic (1988) observed the inverse relation between v_s and Q_s for level of strains greater than 0.001 per cent. These levels are larger than those induced in the material by the seismic noise signal used in this study. In their study, the scatter of the data in the low strain domain did not allow the identification of any trend as a function of the plasticity of the soil.

Therefore, our results suggest that possibly, from *in-situ* measurements, the behaviour observed in laboratory experiments can be extended to lower levels of strain in the material. It is worth noting, that in a similar way, previous studies (e.g. Rubinstein 2011) recently showed that non-linear material behaviour might start at levels of strain lower than previously expected from laboratory analyses.

Since usually no information on the quality factor is available *a priori*, so far many studies rely on numerical simulations of ground motion, which consider quality factors scaled proportionally to velocity. On the other hand, hysteretic damping is often modeled by means of linear viscoelastic approaches such as constant attenuation models. However, these models cannot fully be applied without compromising their reliability as they do not take into account non-linear effects, either on the stiffness, or the damping, which are well-known features of soil dynamics behaviour, meaning that this issue will require future research.

6 CONCLUSIONS

We have presented the results of the application of a novel approach based on the inversion of seismic noise for determining v_s and Q_s at several sedimentary sites in various geological environments. On the basis of well-established techniques for the estimation of the *S*-wave velocity profile through a joint inversion scheme of the surface wave dispersion curves and the H/V spectral ratio, we have confirmed that, by simply adding a few additional calculation steps, the method can provide well-constrained Q_s versus depth estimates. To this regard, an iterative grid-search procedure is performed to find the value of the phase velocity and the frequency-dependent attenuation factor providing the best fit to the data. Differently from previous studies, all v_s and Q_s values have been derived using the same methods, making them directly comparable while avoiding misinterpretation related to different techniques and different frequency ranges analysed.

In contradiction to previous results, a slight inverse correlation between v_s and Q_s was found. Particularly, low Q_s values have been obtained for sandy and gravelly sites for which high *S*-wave velocities have been observed, meaning that a relationship of Q_s with geology seems to be more important than previously thought. We think that this is due to the fact that only unconsolidated material was considered, and that the role of the grain matrix and grain contact should play a major role with respect to these parameters.

However, although uncertainties in the data do not permit a definitive conclusion, these results highlight an issue that deserves greater attention due to importance, for example in hazard calculation and in the estimation and application of path-corrected spectral decay factor κ_0 (e.g. Parolai *et al*. 2015; Pilz & Fäh, 2017). For a more quantitative analysis, it is highly desirable to study sites where additional information is available. Detailed laboratory investigations of petrophysical identification of lithology, porosity, water saturation and permeability linked to measurements of seismic velocities and attenuation under well-defined confining pressure for the various stratigraphic units will be fundamental for linking the various parameters more efficiently. In the future, when done so, such simple and inexpensive methods might contribute to more comprehensive geotechnical investigations, such as soil investigations, which are important for construction engineering, as well as other fields in applied engineering geophysics.

ACKNOWLEDGEMENTS

For the experiments, instruments were provided by the Geophysical Instrumental Pool of the GFZ Potsdam. We are grateful to the field crews and various local people who allowed us to make the measurements in excellent conditions and who provided helpful information on the local site conditions. We thank the two anonymous reviewers and the Editor for their comments and suggestions that have helped us to improve upon the original version of the manuscript.

REFERENCES

Aki, K., 1957. Space and time spectra of stationary stochastic waves, with special reference to microtremors, *Bull. Earthq. Res. Inst.,* **35,** 415–456.

Aki, K., 1965. A note on the use of microseisms in determining the shallow structures of the earth's crust, *Geophysics,* **29,** 665–666.

Aki, K. & Chouet, B., 1975. Origin of coda waves: source, attenuation, and scattering effects, *J. geophys. Res.,* **80,** 3322–3342.

Albarello, D. & Baliva, F., 2009. In-Situ estimates of material damping from environmental noise measurements, in *Increasing Seismic Safety by Combining Engineering Technologies and Seismological Data*, pp. 73–84, eds Mucciarelli, M., Herak, M. & Cassidy, J., Springer, The Netherlands.

Anderson, D., Ben-Menahem, A. & Archambeau, C., 1965. Attenuation of seismic energy in the upper mantle, *J. geophys. Res.,* **70,** 1441–1448.

Assimaki, D., Steidl, J. & Liu, P.C., 2006. Attenuation and velocity structure for site response analyses via downhole seismogram inversion, *Pure appl. Geophys.,* **163,** 81–118.

Bowden, D.C., Tsai, V.C. & Lin, F.C., 2015. Site amplification, attenuation, and scattering from noise correlation amplitudes across a dense array in Long Beach, CA, *Geophys. Res. Lett.,* **42**(5), 1360–1367.

Boxberger, T., Picozzi, M. & Parolai, S., 2011. Shallow geology characterization using Rayleigh and Love wave dispersion curves derived by seismic noise array measurements, *J. appl. Geophys.,* **75,** 345–354.

Campbell, K.W., 2009. Estimates of shear-wave q and k0 for unconsolidated and semi-consolidated sediments in Eastern North America, *Bull. seism. Soc. Am.,* **99,** 2365–2392.

Cupillard, P. & Capdeville, Y., 2010. On the amplitude of surface waves obtained by noise correlation and the capability to recover the attenuation: a numerical approach, *Geophys. J. Int.,* **181**(3), 1687–1700.

Cupillard, P., Stehly, L. & Romanowicz, B., 2011. The one-bit noise correlation: a theory based on the concepts of coherent and incoherent noise, *Geophys. J. Int.,* **184**(3), 1397–1414.

Del Pezzo, E., Ibanez, J., Morales, J., Akinci, A. & Maresca, R., 1995. Measurements of intrinsic and scattering seismic attenuation in the crust, *Bull. seism. Soc. Am.,* **85,** 1373–1380.

Dobry, R. & Vucetic, M., 1988. Dynamic properties and seismic response of soft clay deposits, in *Proc. Int. Symp. Geotechnical Engineering of Soft Soils*, Vol. 2, pp. 51–87, eds Mendoza, M.J. & Montafiez, L., Sociedad Mexicana de Mecanica de Suelos, Ciudad de Mexico.

Fleming, K. *et al.*, 2009. The self-organizing seismic early warning information network (SOSEWIN), *Seismol. Res. Lett.,* **80,** 755–771.

Foti, S., Parolai, S., Albarello, D. & Picozzi, M., 2011. Application of surface-wave methods for seismic site characterization, *Surv. Geophys.,* **32,** 777–825.

Hu, J.F. & Su, Y.J., 1999. Estimation of the quality factor in shallow soil using surface waves, *Acta Seismol. Sin.,* **12**(4), 481–487.

Ishibashi, I. & Zhang, X.J., 1993. Unified dynamic shear moduli and damping ratios of sand and clay, *Soils Found.,* **33,** 182–191.

Ktenidou, O.J., Abrahamson, N.A., Drouet, S. & Cotton, F., 2015. Understanding the physics of kappa (κ): insights from a downhole array, *Geophys. J. Int.,* **203,** 678–691.

Li, X.P., Schott, W. & Rueter, H., 1995. Frequency-dependent Q-estimation of Love-type channel waves and the application of Q-correction to seismograms, *Geophysics,* **60,** 1773–1789.

Liu, X. & Ben-Zion, Y., 2013. Theoretical and numerical results on effects of attenuation on correlation functions of ambient seismic noise, *Geophys. J. Int.,* **194**(3), 1966–1983.

Liu, X., Ben-Zion, Y. & Zigone, D., 2015. Extracting seismic attenuation coefficients from cross-correlations of ambient noise at linear triplets of stations, *Geophys. J. Int.,* **203**(2), 1149–1163.

Menke, W., 1989. *Geophysical Data Analysis: Discrete Inverse Theory*, Vol. 322, Academic Press, Amsterdam, The Netherlands.

Nakahara, H., 2012. Formulation of the spatial autocorrelation (SPAC) method in dissipative media, *Geophys. J. Int.,* **190**(3), 1777–1783.

Nikolaou, S., Go, J., Beyzaei, C.Z., Moss, C. & Deming, P.W., 2012. *Geo-Seismic Design in the Eastern United States: State of Practice,*, Keynote Paper, ASCE GeoCongress, Geotechnical Engineering State of the Art and Practice , Oakland, pp. 828–854.

Ohori, M., Nobata, A. & Wakamatsu, K., 2002. A comparison of ESAC and FK methods of estimating phase velocity using arbitrarily shaped microtremor arrays, *Bull. seism. Soc. Am.,* **92,** 2323–2332.

Okada, H., 2003. *The Microtremor Survey Method*. Geophysical Monograph Series, Vol. 12, Society of Exploration geophysicists.

Ozakin, Y. & Ben-Zion, Y., 2016. Estimating attenuation coefficients and P-wave velocities of the shallow San Jacinto Fault Zone from Betsy gunshots data recorded by a spatially dense array with 1108 sensors, in EGU General Assembly Conference Abstracts, Vienna Austria, Vol. 18, p. 17720.

Parolai, S., 2012. Investigation of site response in urban areas by using earthquake data and seismic noise, in *New Manual of Seismological Observatory Practice 2 (NMSOP-2)*, pp. 1–38, ed. Bormann, P., Potsdam, Germany.

Parolai, S., 2014. Shear wave quality factor qs profiling using seismic noise data from microarrays, *J. Seismol.,* **18,** 695–704.

Parolai, S., Bindi, D., Ansal, A., Kurtulus, A., Strollo, A. & Zschau, J., 2010. Determination of shallow S-wave attenuation by down-hole waveform deconvolution: a case study in Istanbul (Turkey), *Geophys. J. Int.,* **181,** 1147–1158.

Parolai, S., Bindi, D. & Pilz, M., 2015. k0: the role of intrinsic and scattering attenuation, *Bull. seism. Soc. Am.,* **105,** 1049–1052.

Parolai, S., Picozzi, M., Richwalski, S.M. & Milkereit, C., 2005. Joint inversion of phase velocity dispersion and H/V ratio curves from seismic noise recordings using a genetic algorithm, considering higher modes, *Geophys. Res. Lett.,* **32,** L01303, doi: 10.1029/2004GL021115.

Picozzi, M., Parolai, S. & Richwalski, S.M., 2005. Joint inversion of H/V ratios and dispersion curves from seismic noise: estimating the S-wave velocity of bedrock, *Geophys. Res. Lett.,* **32**(11), doi:10.1029/2005GL022878.

Parolai, S., Wang, R. & Bindi, D., 2012. Inversion of borehole weak motion records observed in Istanbul (Turkey), *Geophys. J. Int.,* **188,** 535–548.

Picozzi, M., Milkereit, C., Parolai, S., Jäckel, K.H., Veit, I., Fischer, J. & Zschau, J., 2010. GFZ wireless seismic array (GFZ-WISE), a wireless mesh network of seismic sensors: new perspectives for seismic noise array investigations and site monitoring, *Sensors,* **10,** 3280–3304.

Pilz, M. & Fäh, D., 2017. The contribution of scattering to near-surface attenuation, *J. Seismol.,* 1–19, doi: 10.1007/s10950-017-9638-4.

Pilz, M. & Parolai, S., 2014. Statistical properties of the seismic noise field: influence of soil heterogeneities, *Geophys. J. Int.,* **199,** 430–440.

Prieto, G., Lawrence, J.F. & Beroza, G.C., 2009. Anelastic earth structure from the coherency of the ambient seismic field, *J. geophys. Res.,* **114,** B07303, doi:10.1029/2008JB006067.

Rubinstein, J.L., 2011. Nonlinear site response in medium magnitude earthquakes near Parkfield, California, *Bull. seism. Soc. Am.,* **101,** 275–286.

Snieder & R., 2001. *A Guided Tour of Mathematical Methods for the Physical Sciences*, Cambridge University Press, Cambridge, UK.

Strollo, A., Parolai, S., Jäckel, K.H., Marzorati, S. & Bindi, D., 2008. Suitability of short-period sensors for retrieving reliable H/V peaks for frequencies less than 1 Hz, *Bull. seism. Soc. Am.,* **98,** 671–681.

Tsai, V.C., 2011. Understanding the amplitudes of noise correlation measurements, *J.geophys. Res.,* **116,** B09311, doi: 10.1029/2011JB008483.

Tsai, V.C. & Moschetti, M.P., 2010. An explicit relationship between time-domain noise correlation and spatial autocorrelation (SPAC) results, *Geophys. J. Int.,* **182**(1), 454–460.

Tselentis, G., 1998. Intrinsic and scattering seismic attenuation in W. Greece, *Pure appl. Geophys.,* **153,** 703–712.

Vucetic, M. & Dobry, R., 1991. Effect of soil plasticity on cyclic response, *J. geotech. Eng.,* **117,** 89–107.

Vucetic, M. & Dobry, R., 1988. Degradation of marine clays under cyclic loading, *J. geotech. Eng.,* **114**(2), 133–149.

Weaver, R.L., 2011. On the amplitudes of correlations and the inference of attenuations, specific intensities and site factors from ambient noise, *C. R. Geosci.,* **343**(8), 615–622.

Weemstra, C., Boschi, L., Goertz, A. & Artman, B., 2012. Seismic attenuation from recordings of ambient noise, *Geophysics,* **78,** 1–14.

Weemstra, C., Westra, W., Snieder, R. & Boschi, L., 2014. On estimating attenuation from the amplitude of the spectrally whitened ambient seismic field, *Geophys. J. Int.,* **197**(3), 1770–1788.

Xia, J., Miller, R., Park, C. & Tian, G., 2002. Determining Q of near-surface materials from Rayleigh waves, *J. appl. Geophys.,* **51,** 121–129.

Yokoi, T. & Margaryan, S., 2008. Consistency of the spatial autocorrelation method with seismic interferometry and its consequence, *Geophys. Prospect.,* **56**(3), 435–451.